Supplementary Information (SI) for Journal of Materials Chemistry A.

The cross-boundary catalytic effect of anions and cations enhances the hydrogen storage performance of magnesium-based hydrogen storage materials

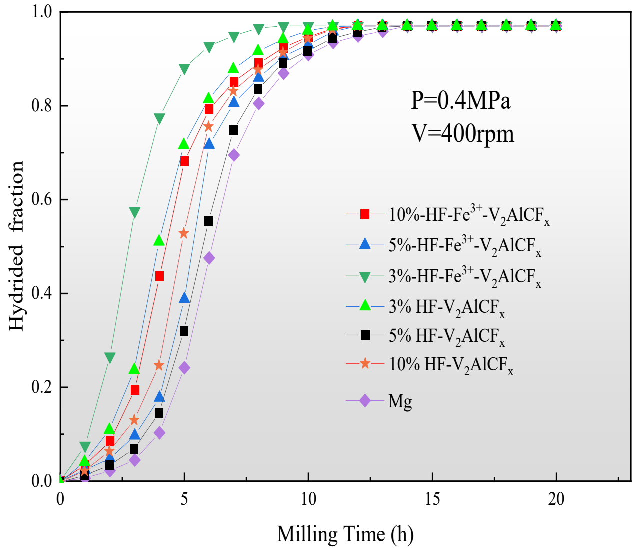

Figure S1 Hydrogenation of Mg and Mg@Fe^{3+}-V_2AlCF_x

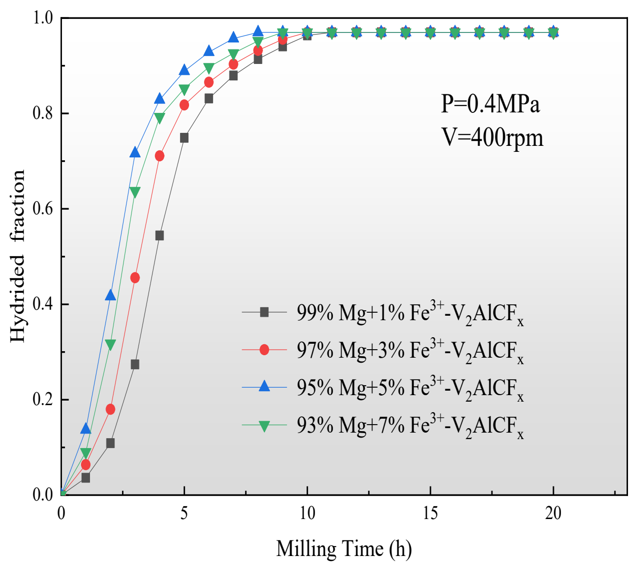

Figure S2 Hydrogenation of Mg+n%Fe^{3+}-V_2AlCF_x

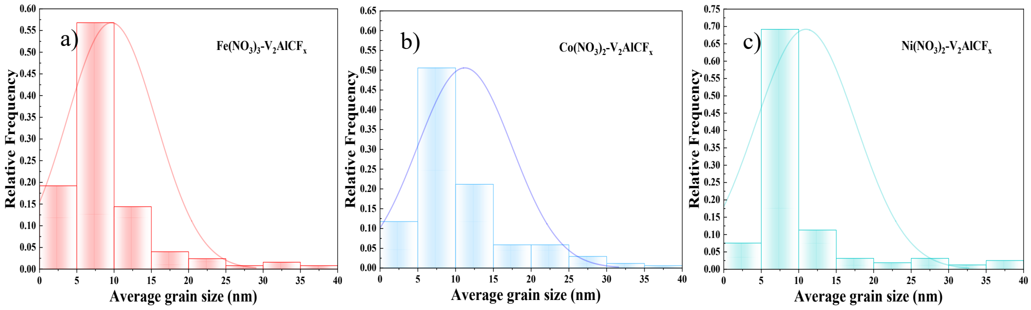

Figure S3 The average grain size of $Fe(NO_3)_3$-V_2AlCF_x, $Co(NO_3)_2$-V_2AlCF_x, and $Ni(NO_3)_2$-V_2AlCF_x

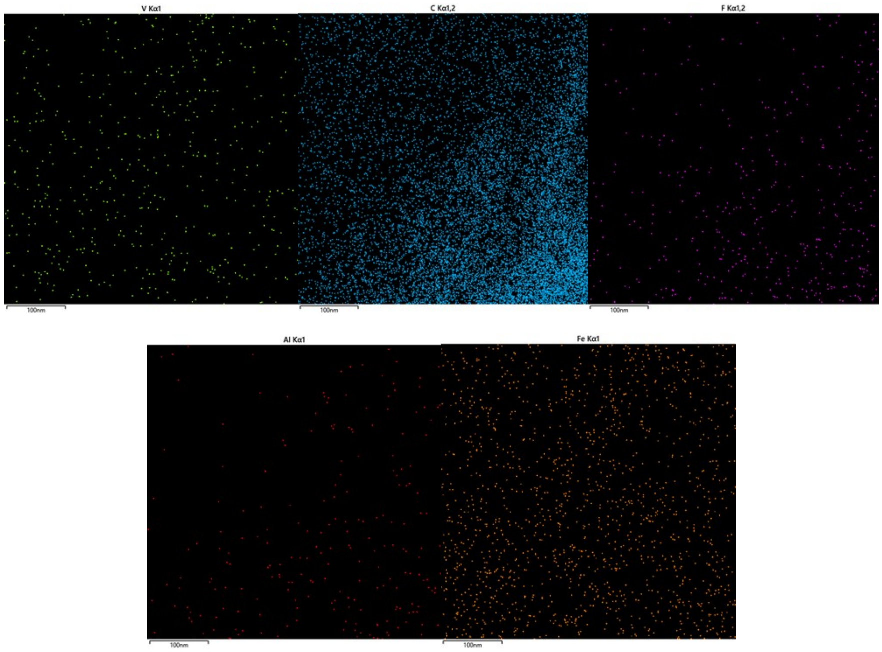

Figure S4 EDS Mappings of $Fe(NO_3)_3$-V_2AlCF_x

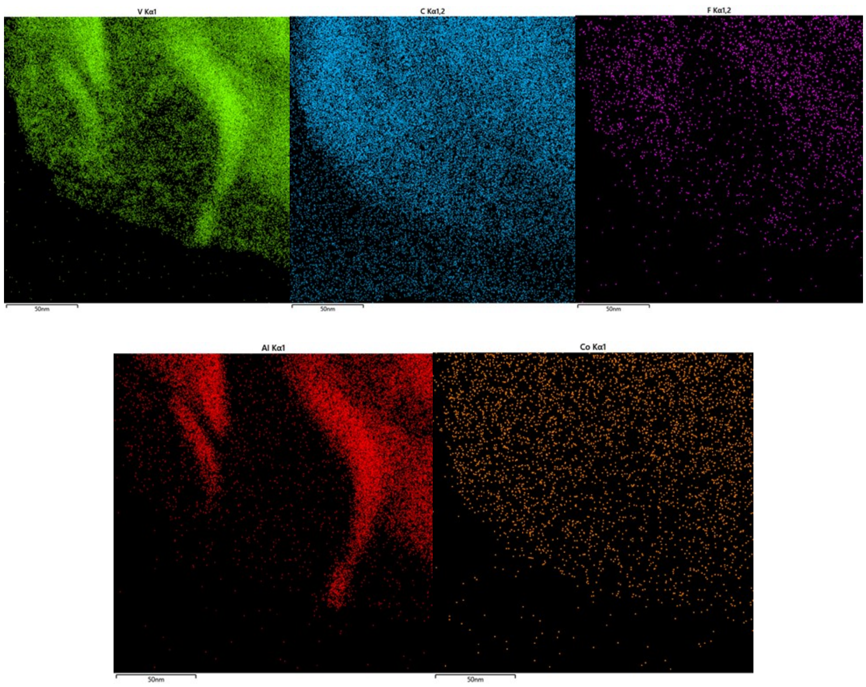

Figure S5 EDS Mappings of $Co(NO_3)_2$-V_2AlCF_x

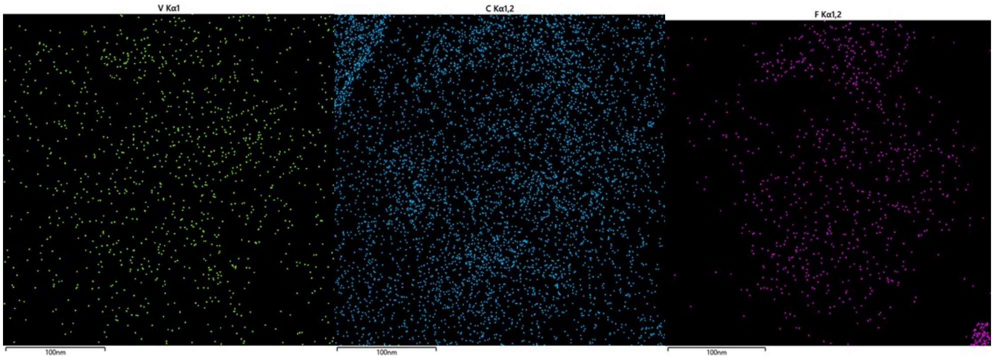

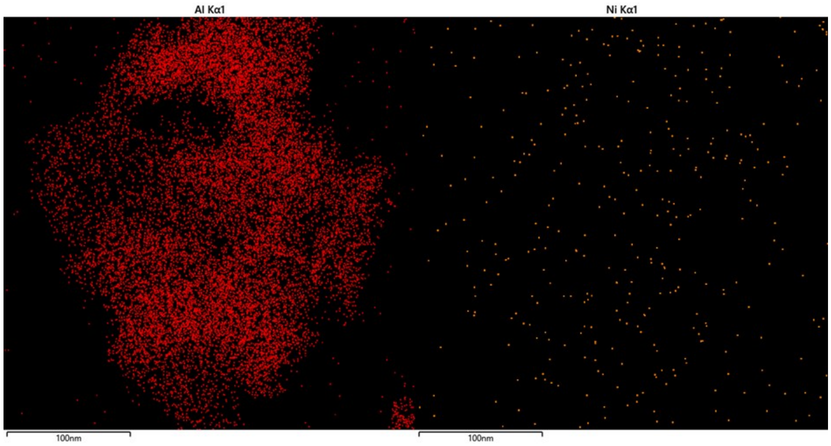

Figure S6 EDS Mappings of $Ni(NO_3)_2$-V_2AlCF_x

Table S1 Values of n, ln(K) and equation of Mg@Fe^{3+}-V_2AlCF_x under 300r/min with a pressure of 0.2 MPa.

P	V	BPR	n	ln（K）	Kinetic equation
0.2MPa	300r/min	120：1	1.79	-3.00	$\alpha = 1 - \exp\left(-4.98 \times 10^{-2} t^{1.89}\right)$
0.2MPa	300r/min	100：1	1.74	-3.30	$\alpha = 1 - \exp\left(-3.69 \times 10^{-2} t^{1.75}\right)$
0.2MPa	300r/min	80：1	1.59	-3.50	$\alpha = 1 - \exp\left(-3.02 \times 10^{-2} t^{1.59}\right)$
0.2MPa	300r/min	60：1	1.46	-3.90	$\alpha = 1 - \exp\left(-2.02 \times 10^{-2} t^{1.46}\right)$

Table S2 Values of n, ln(K) and equation of Mg@Fe^{3+}-V_2AlCF_x under 300r/min with a pressure of 0.4 MPa.

P	V	BPR	n	ln（K）	Kinetic equation
0.4MPa	300r/min	120：1	1.81	-2.60	$\alpha = 1 - \exp\left(-7.43 \times 10^{-2} t^{1.81}\right)$
0.4MPa	300r/min	100：1	1.75	-2.81	$\alpha = 1 - \exp\left(-6.02 \times 10^{-2} t^{1.75}\right)$
0.4MPa	400r/min	80：1	1.73	-2.92	$\alpha = 1 - \exp\left(-5.39 \times 10^{-2} t^{1.73}\right)$
0.4MPa	400r/min	60：1	1.71	-3.34	$\alpha = 1 - \exp\left(-3.54 \times 10^{-2} t^{1.72}\right)$

Table S3 Values of n, ln(K) and equation of Mg@Fe^{3+}-V_2AlCF_x under 400r/min with a pressure of 0.4 MPa.

P	V	BPR	n	ln（K)	Kinetic equation
0.4MPa	400r/min	120：1	1.83	-2.12	$\alpha = 1 - \exp\left(-1.20 \times 10^{-1} t^{1.83}\right)$
0.4MPa	400r/min	100：1	1.78	-2.19	$\alpha = 1 - \exp\left(-1.12 \times 10^{-1} t^{1.75}\right)$
0.4MPa	400r/min	80：1	1.74	-2.28	$\alpha = 1 - \exp\left(-1.02 \times 10^{-1} t^{1.74}\right)$
0.4MPa	400r/min	60：1	1.72	-2.30	$\alpha = 1 - \exp\left(-1.00 \times 10^{-1} t^{1.72}\right)$

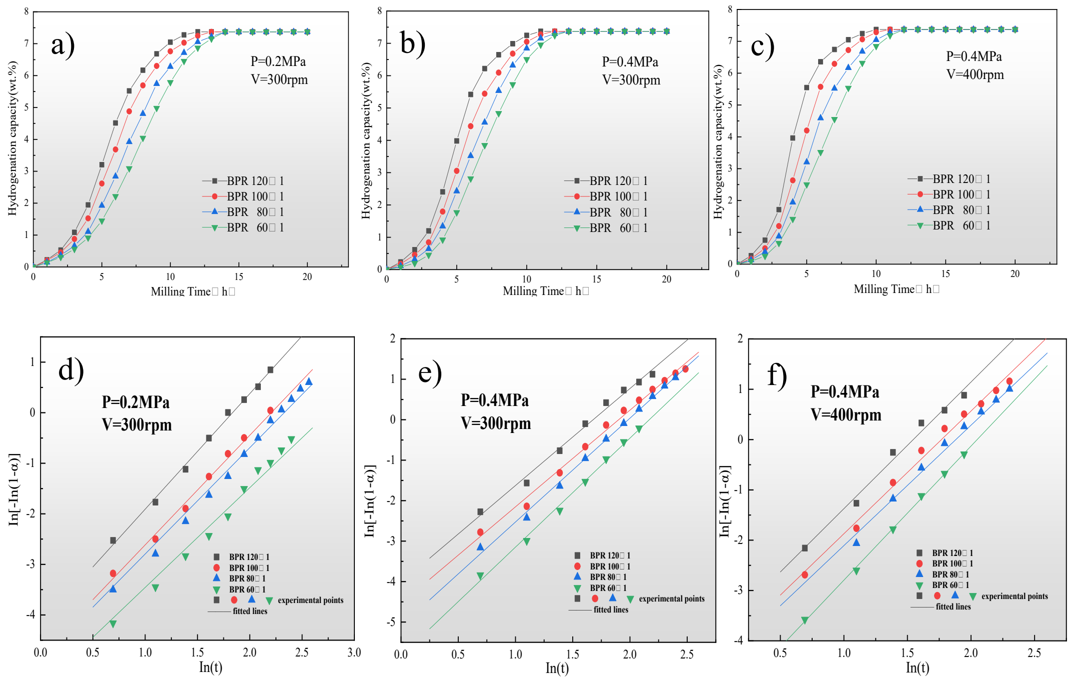

Figure S7 a) Hydrogenation of Mg@Co^{2+}-V_2AlCF_x under various milling conditions, b-d) lnln(1/(1-α)) curves for hydrogenation of Mg@ Co^{2+}-V_2AlCF_x under various milling conditions as a function of ln(t) with linear fitting

Table S4 Values of n, ln(K) and equation of Mg@Co^{2+}-V_2AlCF_x under 300r/min with a pressure of 0.2 MPa.

P	V	BPR	n	ln（K)	Kinetic equation
0.2MPa	300r/min	120：1	2.23	-4.12	$\alpha = 1 - \exp\left(-1.62 \times 10^{-2} t^{2.23}\right)$
0.2MPa	300r/min	100：1	2.17	-4.78	$\alpha = 1 - \exp\left(-8.40 \times 10^{-3} t^{2.17}\right)$
0.2MPa	300r/min	80：1	2.1	-4.90	$\alpha = 1 - \exp\left(-7.45 \times 10^{-3} t^{2.1}\right)$
0.2MPa	300r/min	60：1	1.97	-5.43	$\alpha = 1 - \exp\left(-4.38 \times 10^{-3} t^{1.97}\right)$

Table S5 Values of n, ln(K) and equation of Mg@Co^{2+}-V_2AlCF_x under 300r/min with a pressure of 0.4 MPa.

P	V	BPR	n	ln（K)	Kinetic equation

0.4MPa	300r/min	120：1	2.4	-4.02	$\alpha = 1 - \exp\left(-1.80 \times 10^{-2} t^{2.4}\right)$
0.4MPa	300r/min	100：1	2.38	-4.54	$\alpha = 1 - \exp\left(-1.09 \times 10^{-2} t^{2.38}\right)$
0.4MPa	400r/min	80：1	2.30	-4.60	$\alpha = 1 - \exp\left(-1.00 \times 10^{-2} t^{2.3}\right)$
0.4MPa	400r/min	60：1	2.27	-5.15	$\alpha = 1 - \exp\left(-5.80 \times 10^{-3} t^{2.27}\right)$

Table S6 Values of n, ln(K) and equation of Mg@Co^{2+}-V_2AlCF_x under 400r/min with a pressure of 0.4 MPa.

P	V	BPR	n	ln（K）	Kinetic equation
0.4MPa	400r/min	120：1	2.52	-3.89	$\alpha = 1 - \exp\left(-2.04 \times 10^{-2} t^{2.52}\right)$
0.4MPa	400r/min	100：1	2.44	-4.31	$\alpha = 1 - \exp\left(-1.34 \times 10^{-2} t^{2.44}\right)$
0.4MPa	400r/min	80：1	2.39	-4.50	$\alpha = 1 - \exp\left(-1.11 \times 10^{-2} t^{2.39}\right)$
0.4MPa	400r/min	60：1	2.30	-4.89	$\alpha = 1 - \exp\left(-7.52 \times 10^{-3} t^{2.30}\right)$

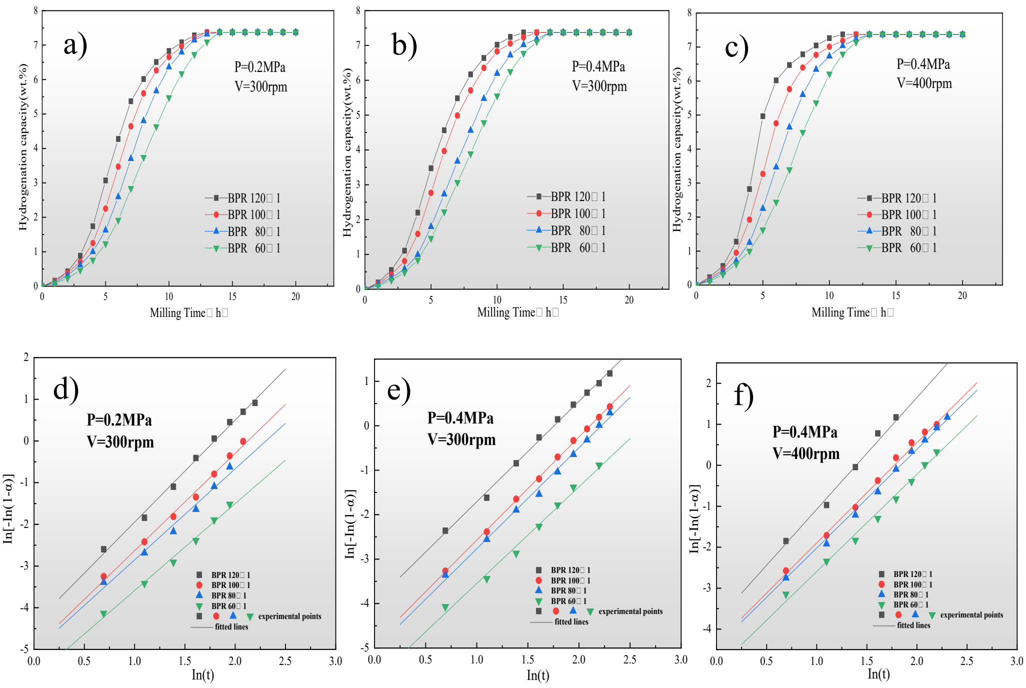

Figure S8 a) Hydrogenation of Mg@Ni^{2+}-V_2AlCF_x under various milling conditions, b-d) lnln(1/(1-α)) curves for hydrogenation of Mg@ Ni^{2+}-V_2AlCF_x under various milling conditions as a function of ln(t) with linear fitting

Table S7 Values of n, ln(K) and equation of Mg@Ni^{2+}-V_2AlCF_x under 300r/min with a pressure of 0.2 MPa.

P	V	BPR	n	ln（K）	Kinetic equation
0.2MPa	300r/min	120：1	2.18	-3.92	$\alpha = 1 - \exp\left(-1.98 \times 10^{-2} t^{2.18}\right)$

0.2MPa	300r/min	100：1	2.08	-4.56	$\alpha = 1 - \exp\left(-1.05 \times 10^{-2} t^{2.08}\right)$
0.2MPa	300r/min	80：1	1.93	-4.65	$\alpha = 1 - \exp\left(-9.56 \times 10^{-3} t^{1.93}\right)$
0.2MPa	300r/min	60：1	1.85	-5.31	$\alpha = 1 - \exp\left(-4.94 \times 10^{-3} t^{1.85}\right)$

Table S8 Values of n, ln(K) and equation of Mg@Ni^{2+}-V_2AlCF_x under 300r/min with a pressure of 0.4 MPa.

P	V	BPR	n	ln（K）	Kinetic equation
0.4MPa	300r/min	120：1	2.26	-3.97	$\alpha = 1 - \exp\left(-1.89 \times 10^{-2} t^{2.26}\right)$
0.4MPa	300r/min	100：1	2.11	-4.50	$\alpha = 1 - \exp\left(-1.11 \times 10^{-2} t^{2.11}\right)$
0.4MPa	400r/min	80：1	2.01	-4.57	$\alpha = 1 - \exp\left(-1.03 \times 10^{-2} t^{2.01}\right)$
0.4MPa	400r/min	60：1	1.89	-5.30	$\alpha = 1 - \exp\left(-4.99 \times 10^{-3} t^{1.89}\right)$

Table S9 Values of n, ln(K) and equation of Mg@Ni^{2+}-V_2AlCF_x under 400r/min with a pressure of 0.4 MPa.

P	V	BPR	n	ln（K）	Kinetic equation
0.4MPa	400r/min	120：1	2.73	-3.80	$\alpha = 1 - \exp\left(-2.23 \times 10^{-2} t^{2.73}\right)$
0.4MPa	400r/min	100：1	2.45	-4.34	$\alpha = 1 - \exp\left(-1.30 \times 10^{-2} t^{2.45}\right)$
0.4MPa	400r/min	80：1	2.42	-4.46	$\alpha = 1 - \exp\left(-1.16 \times 10^{-2} t^{2.42}\right)$
0.4MPa	400r/min	60：1	2.37	-4.97	$\alpha = 1 - \exp\left(-6.94 \times 10^{-3} t^{2.37}\right)$

Table S10 Activation energy of Mg@Fe^{3+}-V_2AlCF_x under the condition of 0.4MPa and 400r/min

P	V	BPR	Ea（KJ/mol）	Average（KJ/mol）
0.4MPa	400 r/min	120:1	16.45	20.26
0.4MPa	400 r/min	100:1	19.54	
0.4MPa	400 r/min	80:1	21.84	
0.4MPa	400 r/min	60:1	23.22	

Table S11 Activation energy of Mg@Fe^{3+}-V_2AlCF_x under the condition of 0.4MPa and 300r/min

P	V	BPR	Ea（KJ/mol）	Average（KJ/mol）

0.4MPa	300 r/min	120:1	19.79	24.47
0.4MPa	300 r/min	100:1	23.59	
0.4MPa	300 r/min	80:1	25.79	
0.4MPa	300 r/min	60:1	28.74	

Table S12 Activation energy of $Mg@Co^{2+}-V_2AlCF_x$ under the condition of 0.4MPa and 400r/min

P	V	BPR	Ea（KJ/mol）	Average（KJ/mol）
0.4MPa	400 r/min	120:1	25.07	30.44
0.4MPa	400 r/min	100:1	29.53	
0.4MPa	400 r/min	80:1	32.82	
0.4MPa	400 r/min	60:1	34.33	

Table S13 Activation energy of $Mg@Co^{2+}-V_2AlCF_x$ under the condition of 0.4MPa and 300r/min

P	V	BPR	Ea（KJ/mol）	Average（KJ/mol）
0.4MPa	300 r/min	120:1	26.61	33.53
0.4MPa	300 r/min	100:1	29.8	
0.4MPa	300 r/min	80:1	36.88	
0.4MPa	300 r/min	60:1	40.81	

Table S14 Activation energy of $Mg@Ni^{2+}-V_2AlCF_x$ under the condition of 0.4MPa and 400r/min

P	V	BPR	Ea（KJ/mol）	Average（KJ/mol）
0.4MPa	400 r/min	120:1	27.08	35.53
0.4MPa	400 r/min	100:1	35.11	
0.4MPa	400 r/min	80:1	38.87	
0.4MPa	400 r/min	60:1	41.08	

Table S15 Activation energy of $Mg@Ni^{2+}-V_2AlCF_x$ under the condition of 0.4MPa and 300r/min

P	V	BPR	Ea（KJ/mol）	Average（KJ/mol)
0.4MPa	300 r/min	120:1	33.16	38.78
0.4MPa	300 r/min	100:1	35.1	
0.4MPa	300 r/min	80:1	41.3	
0.4MPa	300 r/min	60:1	45.57	

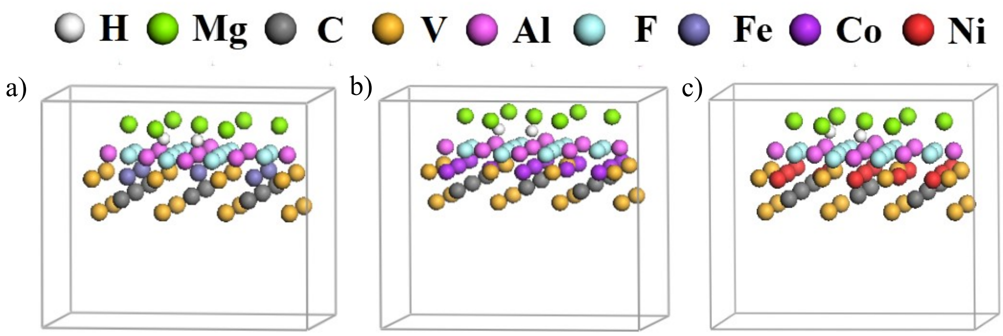

Figure S9 The optimized structures of H_2 adsorption on the a) Mg@Fe^{3+}-V_2AlCF_x, b) Mg@Co^{2+}-V_2AlCF_x and c) Mg@Ni^{2+}-V_2AlCF_x surfaces.

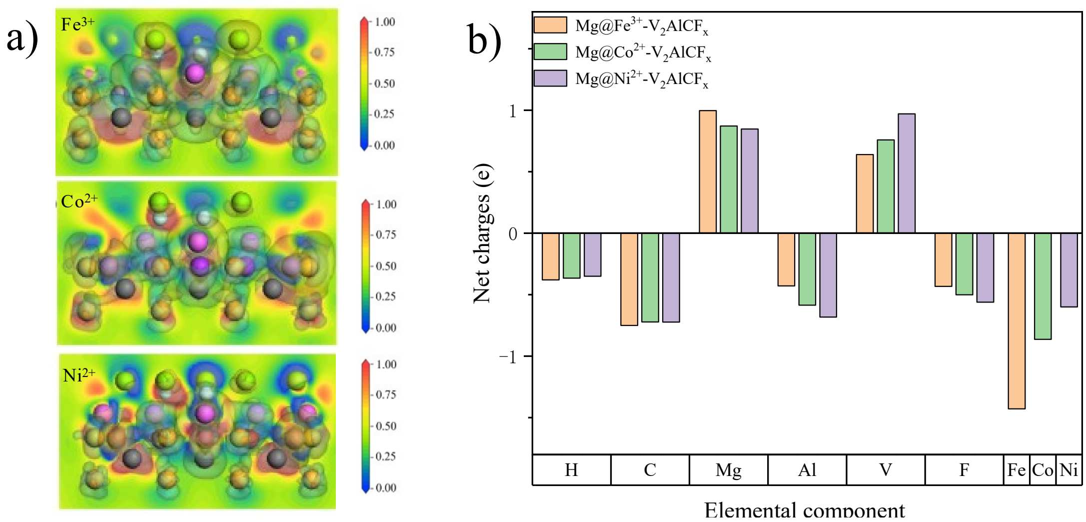

Figure S10 The a) DDC and b) Mulliken's charge of the H_2 adsorption on the Mg@Fe^{3+}-V_2AlCF_x, Mg@Co^{2+}-V_2AlCF_x and Mg@Ni^{2+}-V_2AlCF_x surfaces.

Table S16 The adsorption energy of H_2 on the Mg(0001)@TM^{x+}-V_2AlCF_x surface.

Ea/Ha	Mg@Fe^{3+}-V_2AlCF_x	Mg@Co^{2+}-V_2AlCF_x	Mg@Ni^{2+}-V_2AlCF_x
Top	-0.0085870	-0.0063263	-0.0086272
Bridge	-0.0073517	-0.0075125	-0.0079703
Fcc	**-0.0280089**	-0.0246339	**-0.0214725**

Hcp	-0.0251754	**-0.0256035**	-0.0206573

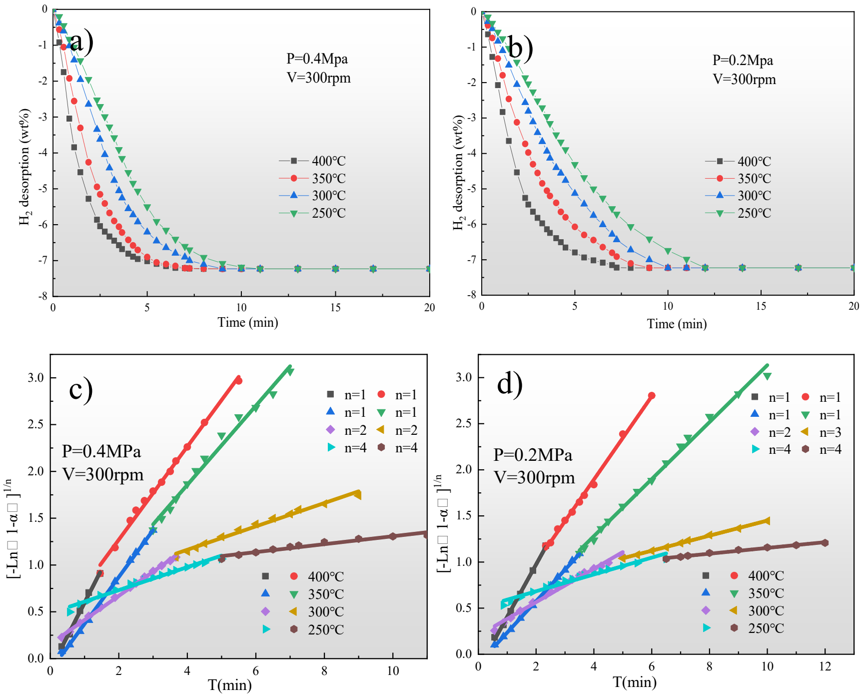

Figure S11 a-b) Isothermal dehydrogenation curves for MgH_2@Ni-V_2AlCF_x under a variety of conditions, c-d) Curves of $[-\ln(1-\alpha)]^{1/n}$ depicting the dehydrogenation process of MgH_2@Ni-V_2AlCF_x as a function of T, accompanied by their corresponding linear fittings.

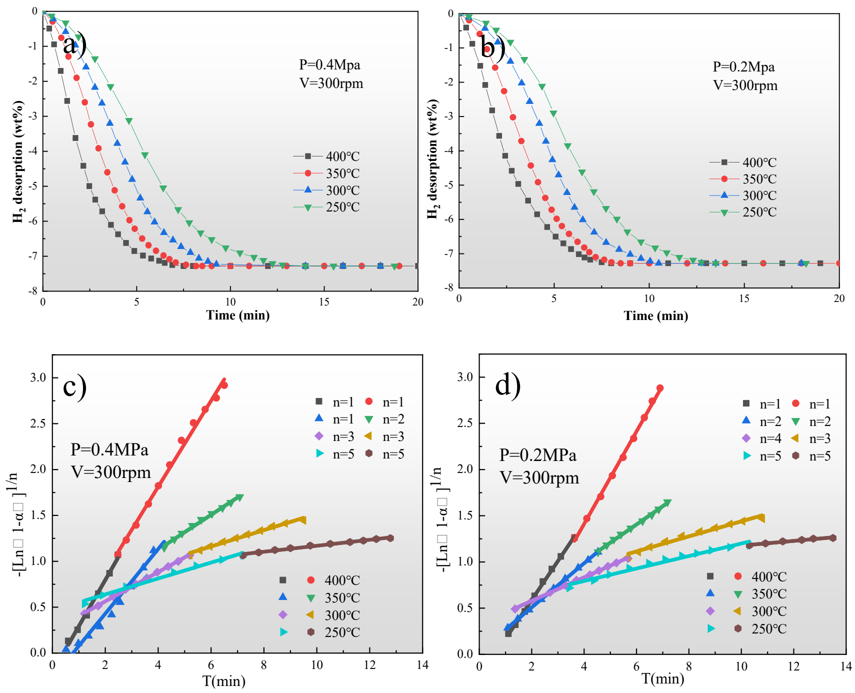

Figure S12 a-b) Isothermal dehydrogenation curves for MgH_2@Co-V_2AlCF_x under a variety of conditions, c-d) Curves of $[-\ln(1-\alpha)]^{1/n}$ depicting the dehydrogenation process of MgH_2@Co-V_2AlCF_x as a function of T, accompanied by their corresponding linear fittings.

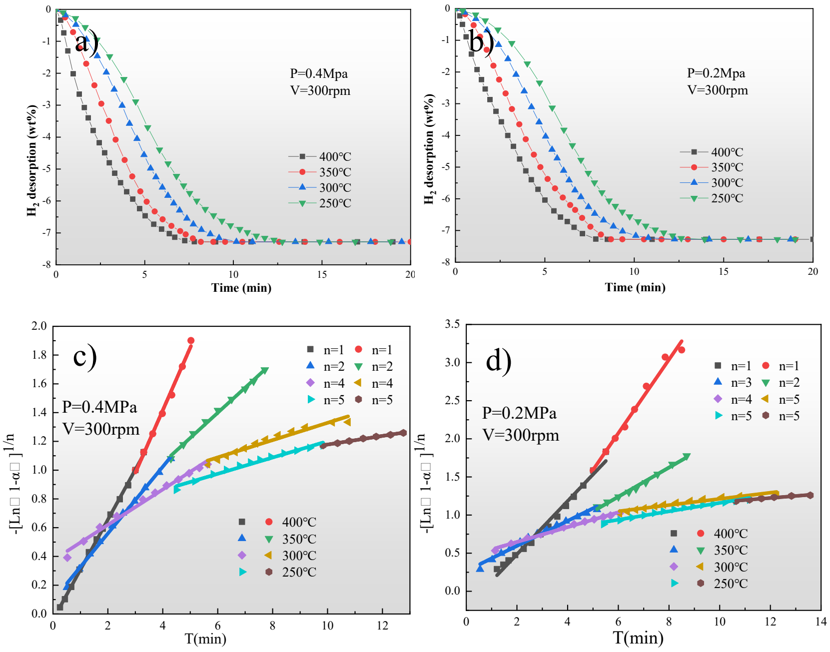

Figure S13 a-b) Isothermal dehydrogenation curves for MgH_2@Fe-V_2C under a variety of conditions, c-d) Curves of $[-\ln(1-\alpha)]^{1/n}$ depicting the dehydrogenation process of MgH_2@Fe-V_2AlCF_x as a function of T, accompanied by their corresponding linear fittings.

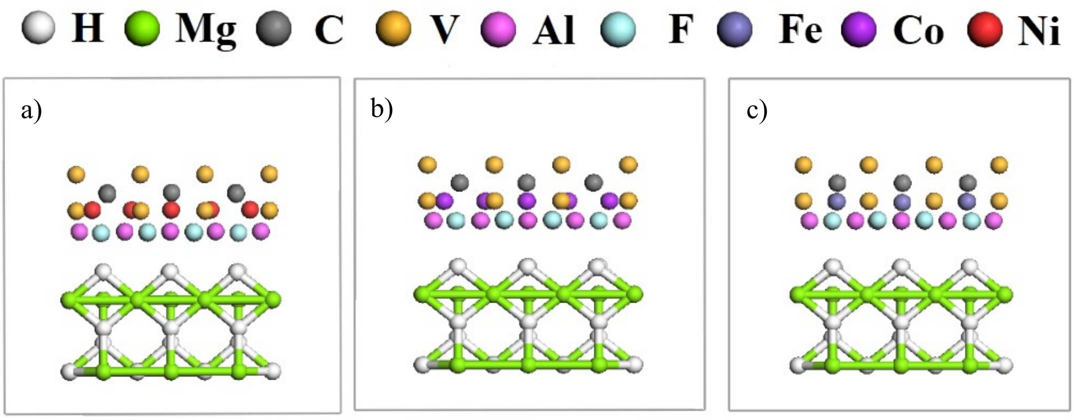

Figure S14 The optimized structures of the a) MgH_2@Fe-V_2AlCF_x, b) MgH_2@Co-V_2AlCF_x and c) MgH_2@Ni-V_2AlCF_x surfaces.

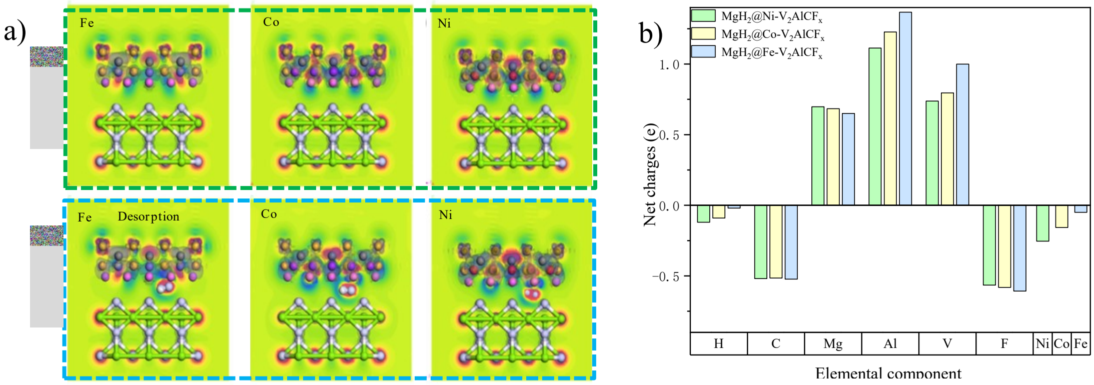

Figure S15 The a) DDC and b) Mulliken's charge of the H_2 desorption on the MgH_2@Fe-V_2AlCF_x, MgH_2@Co-V_2AlCF_x and MgH_2@Ni-V_2AlCF_x surfaces.

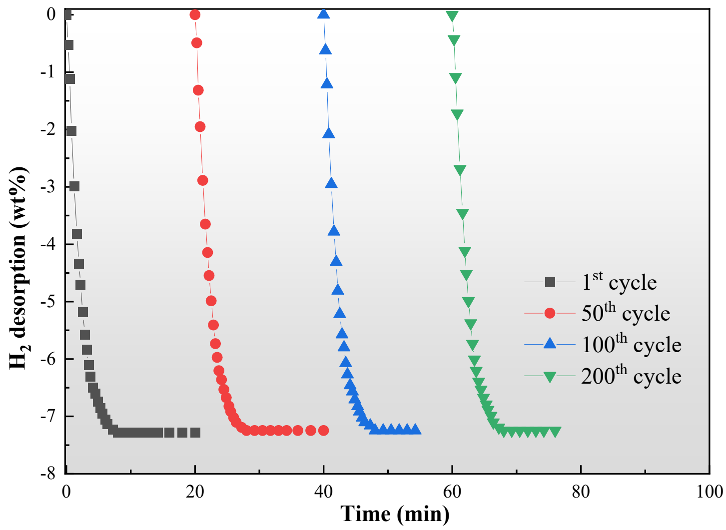

Figure S16 The dehydrogenation kinetics of MgH_2@Fe-V_2AlCF_x during 200 cycles.